analytical chemistry

Article

pubs.acs.org/ac

High-Quantum-Yield Mitochondria-Targeting Near-Infrared Fluorescent Probe for Imaging Native Hypobromous Acid in Living Cells and in Vivo

Xiaojun Liu, Aishan Zheng, Dongrui Luan, Xiaoting Wang, Fanpeng Kong, Lili Tong, Kehua Xu,* and Bo Tang*

College of Chemistry, Chemical Engineering and Materials Science, Collaborative Innovation Center of Functionalized Probes for Chemical Imaging in Universities of Shandong, Key Laboratory of Molecular and Nano Probes, Ministry of Education, Institute of Molecular and Nano Science, Shandong Normal University, Jinan, Shandong 250014, P. R. China

Supporting Information

ABSTRACT: The discovery that hypobromous acid (HOBr) can regulate the activity of collagen IV has attracted great attention. However, HOBr as an important reactive small molecule has hardly ever been studied using a detection method suitable for organisms. Herein, a high-quantum-yield mitochondria-targeting near-infrared (NIR) fluorescent probe for HOBr, **RhSN-mito**, was designed. **RhSN-mito** was easily obtained by the Suzuki cross-coupling reaction. The test results show that **RhSN-mito** can rapidly respond to HOBr with ultrasensitivity and high selectivity. The achievement of ultrasensitivity lies in the high signal-to-noise ratio and the highest fluorescence quantum yield of the reaction product (Φ_F = 0.68) in the near-infrared region, as far as we know. **RhSN-mito** is successfully applied to image native HOBr in mitochondria of HepG2 cells and zebrafish. Thus, **RhSN-mito** is a powerful tool for detecting native HOBr in vivo and is expected to provide a method to further study the physiological and pathological functions related to HOBr.

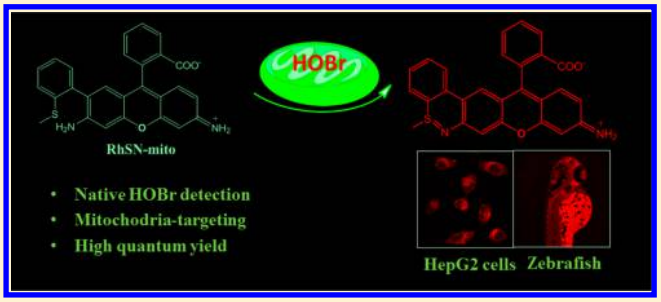

Mitochondria are vital intracellular organelles, involved in many biological processes, including cell signaling, cellular differentiation, cell growth, and triggering of cell apoptosis.[1−5] These processes have a close relationship with reactive oxygen species (ROS).[6] As the primary consumers of cellular oxygen, mitochondria are a major source of cellular reactive ROS including known superoxide anion ($O_2^{\bullet-}$),[7] hydrogen peroxide (H_2O_2),[8] hydroxyl radical ($^{\bullet}OH$),[9] and hypochlorous acid (HOCl).[2] However, it is still unknown whether hypobromous acid (HOBr) is generated in mitochondria.

HOBr is an important ROS very similar to HOCl, in both its structure and formation. In organelles, HOBr and HOCl are generated from a halogen anion (Br^- or Cl^-) and H_2O_2 under the catalysis of heme peroxidase.[10] Recently, more and more mitochondria-targeting fluorescent probes for HOCl have been reported,[11−17] such as the rhodamine thiolactone triphenylphosphonium cation (RSTPP) fluorescent probe[11] and two-photon fluorescent probes that target mitochondria and lysosomes.[12] However, the low plasma level of Br^-, at least 1000-fold lower than that of Cl^-, greatly limits the establishment of the detection method for HOBr.[18] To date, there are only two reversible fluorescent probes for HOBr/Vc (ascorbic acid) and HOBr/H_2S, and a visible fluorescent probe (**BPP**) for HOBr developed in our group has been reported lately.[19−21] The two reported reversible fluorescent probes are not competent for the specific detection of HOBr. **BPP** is the first specific fluorescent probe for native HOBr, yet it cannot target mitochondria in living cells. This means none of the reported fluorescent probes for HOBr are suitable tools to investigate whether HOBr is generated in mitochondria. Consequently, it is of great significance and pressing need to design mitochondria-targeting fluorescent probe to monitor native HOBr in vivo.

In 2014, Hudson and co-workers reported that HOBr can regulate the activity of collagen IV, on the basis of a coupled reaction of hydroxylysine and methionine in the presence of HOBr.[22] Inspired by their work, we design a high-quantum-yield mitochondria-targeting near-infrared (NIR) fluorescent probe (**RhSN-mito**) for imaging native HOBr in vivo. The synthesis process and reaction response to HOBr are displayed in Scheme 1. In the design of the probe structure, we chose rhodamine 110 as a fluorophore and the mitochondria-targeting group. This dye possesses high fluorescence quantum yield, good water-solubility, and a vital property of targeting mitochondria, avoiding the introduction of additional mitochondria-targeting functional groups in the probe molecule,

Received: October 18, 2016
Accepted: January 5, 2017
Published: January 5, 2017

DOI: 10.1021/acs.analchem.6b04094
Anal. Chem. 2017, 89, 1787−1792

Scheme 1. (a) Synthesis Route of RhSN-mito and (b) Proposed Reaction between RhSN-mito and HOBr

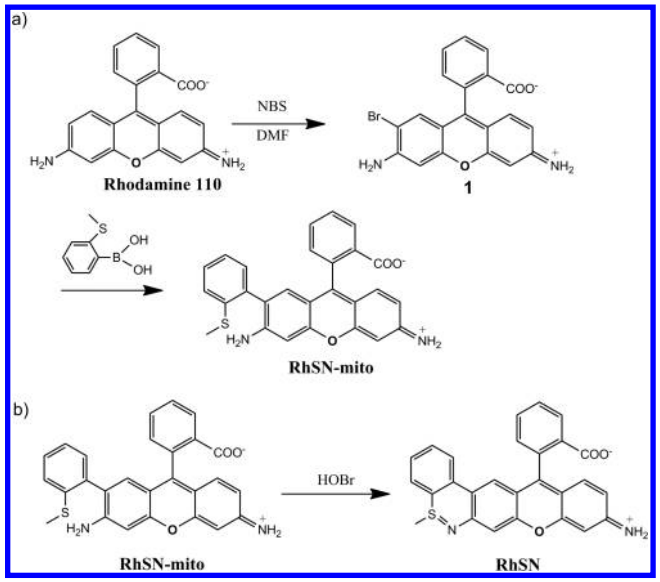

such as a triphenylphosphonium (TPP) moiety or quaternized pyridine moiety.[23] **RhSN-mito** was easily obtained by a Suzuki cross-coupling reaction, and the response of **RhSN-mito** to HOBr, as expected, was rapid, ultrasensitive, and highly selective. The achievement of ultrasensitivity (limit of detection was 20 pM) should be attributed to the structural advantages of the probe and the reaction product: (1) the large emission-wavelength red shift (~100 nm) between **RhSN-mito** and the product **RhSN** improves the signal-to-noise ratio of the detected signal, because the fluorescence signal from **RhSN-mito** itself cannot be found in the noise region, that is to say, the large red-shift can reduce the signal noise; (2) **RhSN** possesses the highest fluorescence quantum yield (Φ_F = 0.68) in the near-infrared region, as far as we know, compared to the products generated by all the other NIR probes reported in the literature.[23−28] On the other hand, the high selectivity to HOBr should be attributed to the difference between HOBr and HOCl in the coupled reaction of the amino group and S-methyl group. According to Hudson and co-workers, HOCl cannot catalyze the cyclization reaction of the amino group and S-methyl group in **RhSN-mito**.[22] As expected, only under the condition of excess **RhSN-mito** was a noncyclic sulfoxide compound formed, but this did not affect the detection of HOBr. The probe was also successfully applied to trace the changes in the HOBr level in the mitochondria of living cells, and we found that the probe can visualize native HOBr in HepG2 cells and zebrafish. Collectively, we believe that **RhSN-mito** is a powerful tool for detecting native HOBr in vitro and in vivo and that it will provide a way to further study the physiological and pathological functions related to HOBr.

EXPERIMENTAL SECTION

Synthesis of RhSN-mito. Rhodamine 110 (200 mg, 0.54 mmol) was introduced in a flask bottle and dissolved in DMF (2 mL). To the resulting solution was added dropwise NBS (86.5 mg, 0.486 mmol) in DMF (1 mL) in an ice bath. The mixture was stirred in an ice bath for approximately 1 h and then heated to room temperature, and stirring was continued for another 6 h and monitored by thin layer chromatography (TLC). After completion, the reaction mixture was washed with dry acetonitrile three times, and the filtrate was concentrated to give Compound **1** as red solid which was used directly in the next step. HRMS *m/z*: calcd. for $C_{20}H_{13}BrN_2O_3$, 409.0182; found, 409.0155 $[M + H]^+$.

A mixture of Compound **1** (100 mg, 0.25 mmol), 2-methylthiophenylboronic acid (126 mg, 0.75 mmol), tetrabutyl ammonium bromide (8.1 mg, 0.025 mmol), and 1,1′-bis(diphenylphosphino) ferrocene-palladium(II) chloride dichloromethane complex (20 mg, 0.025 mmol) was dissolved in 15 mL of toluene. To the resulted mixture were added ethanol (8 mL) and K_2CO_3 (4 mL, 4 M). The resulting solution was heated to 80 °C and stirred for 24 h under Ar atmosphere and monitored by thin layer chromatography (TLC). After completion, the reaction mixture was cooled to room temperature, filtered, and concentrated. The crude product was purified by neutral alumina column chromatography (methanol/dichloromethane = 1:10, v/v) to provide the desired product as red yellow solid (33.9 mg, 30%). HRMS *m/z*: calcd. for $C_{20}H_{20}N_2O_3S$, 453.1267; found, 453.1248 $[M + H]^+$. ^1H NMR (400 MHz, DMSO-d_6, δ): 2.36 (s, 3H), 5.18 (s, 2H), 5.91 (s, 2H), 6.11 (s, 1H), 6.34−6.57 (m, 3H), 6.45 (d, J = 8 Hz, 1H), 7.21−7.32 (m, 3H), 7.46 (s, 2H), 7.69−7.79 (m, 2H), 7.99 (d, J = 8 Hz, 1H). ^{13}C NMR (100 MHz, DMSO-d_6, δ): 15.1, 99.5, 100.5, 110.8, 111.9, 125.7, 126.0, 128.3, 128.9, 129.2, 130.3, 131.4, 135.2, 139.9, 150.7, 152.6, 153.6, 169.3.

Preparation of HOBr and $^-$OBr. *Preparation of HOBr.* Liquid bromine (100 μL) was dissolved in ultrapure water (15 mL), then titrated with $AgNO_3$ solution in an ice bath to the colorless end point, and then filtered. Lambert−Beer's law (eq 1) was used to calculate the concentration of HOBr (ε_{260} = 160 L mol^{-1} cm^{-1}).

Preparation of $^-$OBr. Sodium hydroxide (1.1700 g) was dissolved in ultrapure water (10 mL), and then to this solution cooled in an ice bath was added liquid bromine (386.66 μL), dropwise. The Lambert−Beer's law (eq 1) was used to calculate the concentration of $^-$OBr (ε_{329} = 332 L mol^{-1} cm^{-1}).

Preparation of 50 μM HOBr in a Specified pH. To 2 mL of HEPES solution of specified pH value (2, 4, 6, 8, 10, and 12) was added a certain amount of the stock solution of HOBr, ensuring the absorbance value which equaled that of 50 μM HOBr, according to the Lambert−Beer's law (eq 1, ε_{260} = 160 L mol^{-1} cm^{-1}). To evaluate the effect of pH on fluorescence intensity of **RhSN-mito** toward HOBr, a final concentration of 6 μM **RhSN-mito** was added to the solution of 50 μM HOBr in 2 mL of HEPES of specified pH value and the fluorescence intensities were tested.

Lambert−Beer's law:

$$A = \varepsilon bc \quad (1)$$

where A is the absorbance of HOBr or $^-$OBr, ε is molar extinction coefficient, b is the path length, b = 1 cm, and c is the concentration of HOBr or $^-$OBr.

Determination of Fluorescence Quantum Yield. Fluorescence quantum yield was determined by using Cy5.5 (Φ_F = 0.28 in PBS) as a fluorescence standard. For measurement of the fluorescence quantum yield of **RhSN**, the solution of the product was adjusted to an absorbance of ca. 0.05. The emission spectra were recorded using the maximal excitation wavelength, and the integrated areas of the fluorescence-corrected spectra were measured. The fluorescence quantum yield was obtained by comparing the area under the emission spectrum of the test samples with that of a

DOI: 10.1021/acs.analchem.6b04094
Anal. Chem. 2017, 89, 1787−1792

solution of Cy5.5 (Φ_F = 0.28 in PBS). The fluorescence quantum yield was calculated using eq 2.

$$\Phi_{F(X)} = \Phi_{F(S)}(A_S F_X / A_X F_S)(n_X / n_S)^2 \quad (2)$$

where Φ_F is the fluorescence quantum yield, A is the absorbance at the excitation wavelength, F is the area under the corrected emission curve, and n is the refractive index of the solvents used. Subscripts S and X refer to the standard and to the unknown, respectively.

Confocal Fluorescence Imaging. HepG2 cells were cultured in Dulbecco's modified Eagle's medium (DMEM) with 10% FBS under 10% CO_2, 1% penicillin, and 1% streptomycin at 37 °C (w/v) in a 5% CO_2/95% air incubator. HepG2 cells and HL-7702 cells were grown on confocal dishes. Cells were washed three times with PBS buffer (pH 7.4). Then, the cells were imaged immediately using a confocal microscope with an objective lens (×40). Excitation of probe-treated cells at 633 nm was performed using an argon laser, and the emitted light was collected with a META detector between 650 and 750 nm.

Static confocal images of zebrafish were collected on a Leica Laser Scanning Confocal using a 10× objective. Zebrafish embryos were grown in normal media and were divided into different groups. Embryos were visualized at 72 h after fertilization. Excitation of probe-treated fish at 633 nm was performed using an argon laser, and the emitted light was collected with a META detector between 650 and 750 nm.

MTT Assay. HepG2 cells (1×10^6 cells/well) were dispersed within 96-well microtiter plates with 200 μL per well. Plates were maintained at 37 °C in a 5% CO_2/20% O_2 air incubator for 24 h. After the supernate was discarded, the HepG2 cells were incubated with **RhSN-mito** of different concentrations (0, 10, 20, 100, 200, 300, 500 μM) for another 2 h. The HepG2 cells incubated with the culture medium served as the blank control. With the supernate removed, 100 μL MTT solutions (0.5 mg mL^{-1} in PBS) were added to each well away from light. After 4 h, the remaining MTT solution was removed, and 150 μL of DMSO was added to each well to dissolve the formed formazan crystals. The absorbance was measured at 490 nm with the microplate reader. The experiment was repeated three times, and the data are shown as the mean ± SD.

RESULTS AND DISCUSSION

RhSN-mito was synthesized according to Scheme 1, and the structure was confirmed by HRMS, ^{1}H NMR, and ^{13}C NMR (see Experimental Section). As shown in Figure 1a, the excitation and emission peaks of the probe are located at 495 and 530 nm, respectively. The reaction product of **RhSN-mito** with HOBr displays excitation and emission maxima in the NIR region at 624 and 663 nm, respectively. The addition of HOBr triggers the formation of sulfilimine, resulting in both the excitation and emission spectra exhibiting a large redshift of approximately 100 nm, and the fluorescence quantum yield of the reaction product is up to 0.68, which greatly improves the signal-to-noise ratio and the detection sensitivity.

Subsequently, the fluorescence measurement conditions were optimized, and the optimized concentrations of **RhSN-mito** were 6 μM (Figure S1). Given that the pH has a significant effect on the performance of the fluorescent probe, the fluorescent intensities of the product in HEPES buffers with different pH values ranging from 2 to 12 were then evaluated.

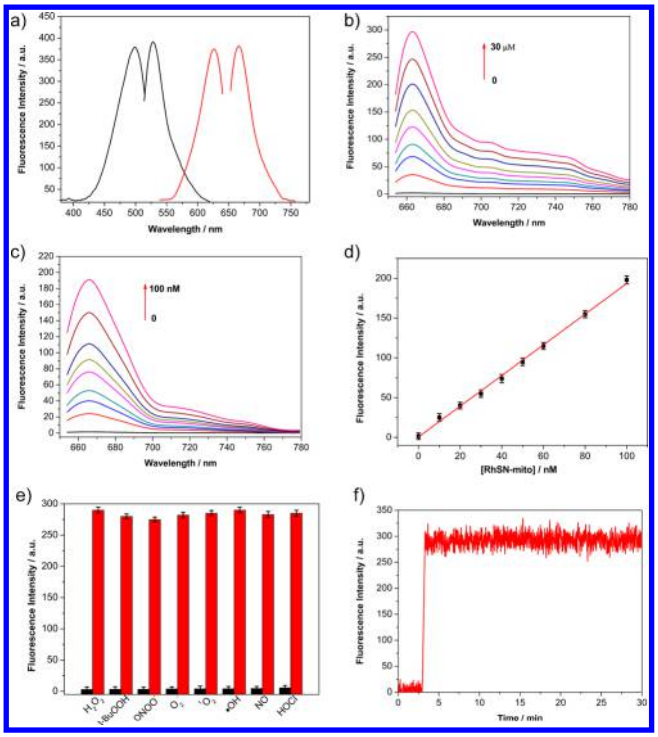

Figure 1. (a) Excitation and emission spectra of **RhSN-mito** (black) and the product of **RhSN-mito** with HOBr (red). (b) Fluorescence intensities of **RhSN-mito** (6 μM) treated with increasing concentrations of HOBr in HEPES (10 mM, pH 7.4, 0.3% DMSO as a cosolvent). The concentration range of HOBr was 0−30 μM; slit widths: 10/20 nm. (c) Fluorescence intensities of **RhSN-mito** (6 μM) treated with increasing concentrations of HOBr in HEPES (10 mM, pH 7.4, 0.3% DMSO as a cosolvent). The concentration range of HOBr was 0−100 nM; slit widths: 20/20 nm. (d) Linear correlation between fluorescence intensities and concentrations of HOBr in the range of 0−100 nM. (e) Selectivity of **RhSN-mito** (6 μM) toward HOBr against various ROSs: 0.5 mM for H_2O_2, *t*-BuOOH, $ONOO^-$, $O_2^{\bullet-}$, $^1O_2$, $^\bullet$OH, NO, 200 μM for HOCl, and 30 μM for HOBr; slit widths: 10/20 nm. (f) Time course of the fluorescence intensities of **RhSN-mito** (6 μM) to HOBr (30 μM) in HEPES (10 mM, pH 7.4, 0.3% DMSO as a cosolvent); slit widths: 10/20 nm; operating voltage: 600 V; $\lambda_{ex}/\lambda_{em}$ = 624/663 nm.

After HOBr was added, remarkable fluorescence enhancements were observed over a wide pH range (pH 2−12) without significant variances (Figure S2), implying that **RhSN-mito** could function properly in living cells, especially in mitochondria.

The fluorescence responses of **RhSN-mito** (6 μM) to HOBr were investigated in HEPES 7.4 (10 mM) at 37 °C (λ_{ex} = 624 nm). Figure 1b,c shows that the fluorescence intensity of the reaction product increased in a dose-dependent manner over a wide concentration range of HOBr. Figure 1d depicts the good linearity between the fluorescence intensity and the concentration of HOBr in the range of 0 to 100 nM. The regression equation was F = 0.64 + 1.94 [HOBr] nM, with a linear coefficient of 0.9975. The limit of detection (3S/m) was determined to be as low as 20 pM, which makes the probe feasible for monitoring the endogenous HOBr. To the best of our knowledge, **RhSN-mito** is the first NIR fluorescent probe capable of the ultrasensitive detection of HOBr at the picomolar level (Table S1).

To inspect whether **RhSN-mito** could specifically monitor HOBr in the complicated intracellular environment, we tested

DOI: 10.1021/acs.analchem.6b04094
Anal. Chem. 2017, 89, 1787−1792

its ability to discriminate between HOBr and various bioanalytes, such as competing ROS, RNS, and relevant biological substances. As shown in Figure 1e, **RhSN-mito** did not display an obvious fluorescence increase in the presence of other ROS, including HOCL, H_2O_2, peroxynitrite ($ONOO^-$), $O_2^{\bullet-}$, singlet oxygen ($^1O_2$), $^{\bullet}OH$, nitric oxide (NO), and TBHP. The metal ions and amino acids present in the living cells had little interferences (Figure S3). Furthermore, after HOBr reacted with **RhSN-mito**, the addition of various reductants caused little decrease in the fluorescence intensities (Figure S4), confirming the high stability of the reaction product. Figure 1f depicts the rapid response of **RhSN-mito** toward HOBr. The fluorescence intensity increased instantly upon the addition of HOBr into the probe solution and was stable for at least 20 min. Additionally, an MTT assay was performed in HepG2 cells (Figure S5), and the IC_{50} value was 650 μM, indicating the low toxicity of **RhSN-mito**. A photobleaching test showed that the reaction product is highly resistant to photobleaching (Figure S6). Collectively, these results indicate that **RhSN-mito** is an excellent fluorescence probe for HOBr and is ideal for specifically detecting native HOBr in living cells and in vivo.

To elucidate the response mechanism of **RhSN-mito** to HOBr, the fluorescence changes of **RhSN-mito** in the presence of HOBr, $^-$OBr, and HOCl were particularly examined (Figure S7). HOBr solution was prepared with Br_2 titrated by $AgNO_3$, and NaOBr solution was obtained from NaOH titrated by Br_2. As shown in Figure S7, the product of **RhSN-mito** with HOBr exhibited a robust increase in the fluorescence intensity at 663 nm, while $^-$OBr and HOCl did not trigger any obvious fluorescence fluctuation at 663 nm. Accordingly, the reaction mechanisms for the response of **RhSN-mito** to HOBr and HOCl were proposed (Scheme 2 and S1), which were in

Scheme 2. Proposed Reaction Mechanism for the Response of RhSN-mito to HOBr

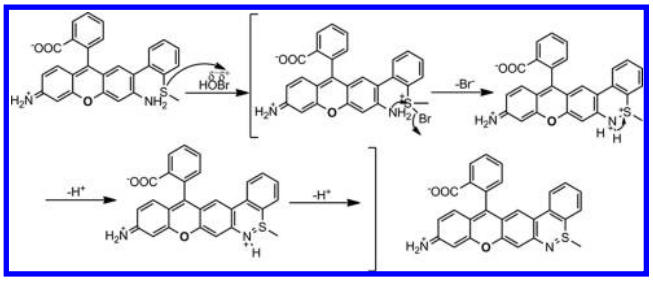

accord with the reported behaviors of HOBr and HOCl.[22] It is HOBr rather than $^-$OBr or HOCl that catalyzes the cyclization reaction of the amino group and the S-methyl group in **RhSN-mito**. In detail, HOBr, converted from Br^-, formed a bromosulfonium-ion intermediate that energetically selects for this cyclization reaction.

Next, we examine the mitochondria-targeting performance of **RhSN-mito**. The colocalization experiments were conducted by costaining HepG2 cells with Mito Tracker Green (a typical commercially available mitochondrial tracker) and **RhSN-mito**. The fluorescence of **RhSN-mito** from the costained cells in the presence of HOBr (Figure 2b) overlaid well with that of Mito Tracker Green (Figure 2a), as shown in the merged image (Figure 2c). The changes in the intensity profiles of the linear regions of interest (ROIs) (**RhSN-mito** and Mito Tracker Green costaining) were synchronous (Figure 2e,f). The

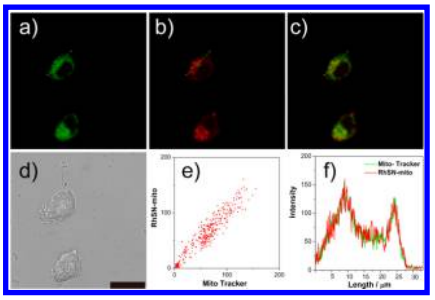

Figure 2. Fluorescence images of mitochondria in HepG2 cells. HepG2 cells were incubated with Mito Tracker Green (500 nM) and **RhSN-mito** (50 μM), respectively, for 30 min and subsequently incubated with HOBr (100 μM) for 30 min. (a) Emission from the green channel (Mito Tracker Green, λ_{ex} = 488 nm, λ_{em} = 500–600 nm), (b) emission from the red channel (**RhSN-mito**, λ_{ex} = 633 nm, λ_{em} = 650–750 nm), (c) merged image of images (a) and (b), (d) corresponding brightfield image, (e) intensity correlation plot of **RhSN-mito** and Mito Tracker Green, and (f) intensity profile of ROIs across HepG2 cells. Scale bar = 25 μm.

colocalization was qualified using Pearson's sample correlation factors. A high Pearson's coefficient of 0.95 and an overlap coefficient of 0.94 are obtained, confirming that **RhSN-mito** was specifically located in the mitochondria of the living HepG2 cells.

Then, **RhSN-mito** was used to detect HOBr in living cells under physiological conditions. As shown in Figure 3b,d, with

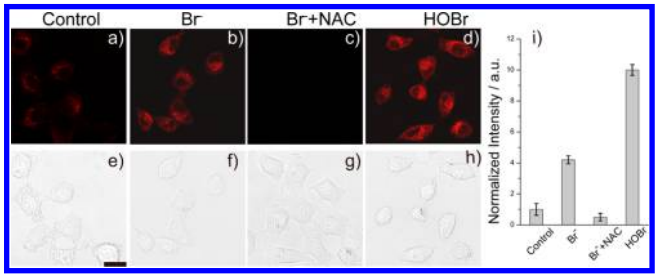

Figure 3. Fluorescence images of HepG2 cells incubated with **RhSN-mito** (50 μM) for 30 min and subsequently incubated for 30 min with (a) nothing as a control, (b) NaBr (100 μM), (c) NaBr (100 μM) plus NAC (20 μM), and (d) HOBr (100 μM), respectively. (e–h) Correspond to brightfield images of (a) to (d). (i) Normalized fluorescence intensity of cells in panels (a) to (d). λ_{ex} = 633 nm, λ_{em} = 650–750 nm, scale bar = 25 μm.

Br^- and HOBr stimulation, the fluorescence intensity of the HepG2 cells was greatly enhanced, and the fluorescence response could largely be inhibited by NAC (a scavenger of HOBr) (Figure 3c). These results demonstrate that **RhSN-mito** is capable of monitoring the exogenous HOBr in HepG2 cells. Additionally, it is worth noting that a weak fluorescence signal was observed in HepG2 cells treated only with **RhSN-mito** (Figure 3a,i). It was inferred that **RhSN-mito** due to its ultrasensitivity could detect the native HOBr in living cells without stimulation. Subsequently, an experiment by pretreating cells with and without NAC was carried out to verify this inference. As shown in Figure 4, the fluorescence-inhibiting effect of NAC was observed in both HepG2 and HL-7702 cells, further supporting the idea that the fluorescence of the living cells incubated only with **RhSN-mito** arises from the native HOBr. Moreover, it was observed that the fluorescence signal

DOI: 10.1021/acs.analchem.6b04094
Anal. Chem. 2017, 89, 1787–1792

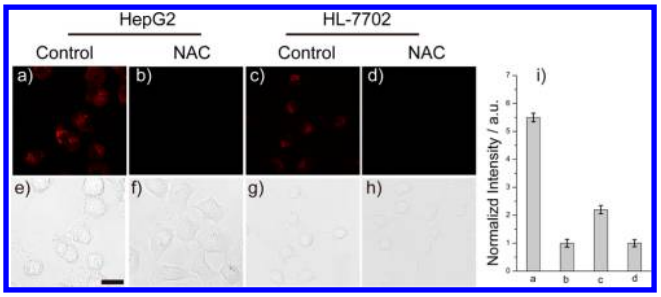

Figure 4. Fluorescence imaging of native HOBr. (a) HepG2 cells incubated with **RhSN-mito** (50 μM) for 30 min, (b) HepG2 cells incubated with NAC (20.0 μM) for 30 min and then with **RhSN-mito** (50.0 μM) for 30 min, (c) HL-7702 cells incubated with **RhSN-mito** (50 μM) for 30 min, (d) HL-7702 cells incubated with NAC (20.0 μM) for 30 min and then with **RhSN-mito** (50.0 μM) for 30 min. (e–h) Correspond to bright-field images of (a) to (d). (i) Normalized fluorescence intensities of cells in panels (a) to (d). λ_{ex} = 633 nm, λ_{em} = 650–750 nm, scale bar = 25 μm.

from HepG2 cells was brighter than that of HL-7702 cells subjected to the same treatment.

Finally, **RhSN-mito** was applied to image HOBr in living animals. Zebrafish was chosen as the bioassay model. Figure 5b

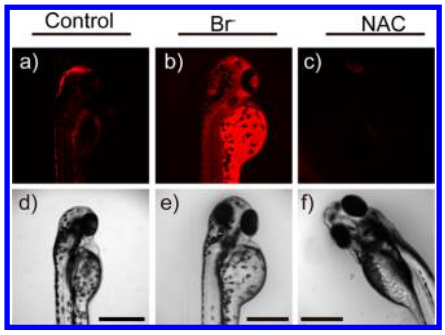

Figure 5. In vivo fluorescence imaging of HOBr in zebrafish embryos developed to 71 h. (a) Zebrafish fed with **RhSN-mito** for 30 min (50.0 μM), (b) zebrafish fed with Br^- (100 μM) for 30 min and then fed with **RhSN-mito** (50.0 μM) for 30 min, and (c) zebrafish incubated with NAC (20.0 μM) for 30 min and then with **RhSN-mito** (50.0 μM) for 30 min. (d–f) Correspond to bright-field images of (a–c). λ_{ex} = 633 nm, λ_{em} = 650–750 nm, scale bar = 500 μm.

shows that the fluorescence intensity significantly increased with the feeding of Br^-. A comparison between Figure 5a,c indicates that **RhSN-mito** could visualize native HOBr in zebrafish. These fluorescence images prove that HOBr can be generated from Br^- in zebrafish, which is in accord with previously reported results.[29] Thus, **RhSN-mito** is a powerful tool for detecting HOBr in vivo.

CONCLUSIONS

In conclusion, a high-quantum-yield mitochondria-targeting NIR fluorescent probe for HOBr, **RhSN-mito**, has been developed on the basis of a specific cyclization reaction. The probe can respond promptly to HOBr with ultrasensitivity, and the limit of detection is as low as 20 pM. This probe is able to target mitochondria and monitor the native HOBr in HepG2 cells and zebrafish. Overall, **RhSN-mito** is an ideal tool for the further study of the physiological and pathological roles of HOBr.

ASSOCIATED CONTENT

Supporting Information

The Supporting Information is available free of charge on the ACS Publications website at DOI: 10.1021/acs.analchem.6b04094.

Materials and instruments, supporting figures and images (PDF)

AUTHOR INFORMATION

Corresponding Authors

*E-mail: tangb@sdnu.edu.cn. Tel.: +86 0531-86180010. Fax: +86 0531-86180017.

*E-mail: xukehua@sdnu.edu.cn. Tel.: +86 0531-86180010. Fax: +86 0531-86180017.

ORCID

Bo Tang: 0000-0002-8712-7025

Author Contributions

All authors have given approval to the final version of the manuscript.

Notes

The authors declare no competing financial interest.

ACKNOWLEDGMENTS

This work was supported by 973 Program (2013CB933800) and National Natural Science Foundation of China (21390411, 21535004, 21275092, 21575081, and 21507075).

REFERENCES

(1) Xiao, H.; Li, P.; Zhang, W.; Tang, B. *Chem. Sci.* **2016**, *7*, 1588–1593.
(2) Hoye, A. T.; Davoren, J. E.; Wipf, P.; Fink, M. P.; Kagan, V. E. *Acc. Chem. Res.* **2008**, *41*, 87–97.
(3) Kroemer, G.; Galluzzi, L.; Brenner, C. *Physiol. Rev.* **2007**, *87*, 99–163.
(4) Hajnóczky, G.; Csordás, G.; Das, S.; Garcia-Perez, C.; Saotome, M.; Sinha Roy, S.; Yi, M. *Cell Calcium* **2006**, *40*, 553–560.
(5) Green, D. R. *Cell* **1998**, *94*, 695–698.
(6) Fulda, S.; Galluzzi, L.; Kroemer, G. *Nat. Rev. Drug Discovery* **2010**, *9*, 447–464.
(7) Li, P.; Liu, L.; Xiao, H.; Zhang, W.; Wang, L.; Tang, B. *J. Am. Chem. Soc.* **2016**, *138*, 2893–2896.
(8) Dickinson, B. C.; Lin, V. S.; Chang, C. J. *Nat. Protoc.* **2013**, *8*, 1249–1259.
(9) Zhuang, M.; Ding, C.; Zhu, A.; Tian, Y. *Anal. Chem.* **2014**, *86*, 1829–1836.
(10) Weiss, S. J.; Test, S. T.; Eckmann, C. M.; Roos, D.; Regiani, S. *Science* **1986**, *234*, 200–203.
(11) Zhou, J.; Li, L.; Shi, W.; Gao, X.; Li, X.; Ma, H. *Chem. Sci.* **2015**, *6*, 4884–4888.
(12) Yuan, L.; Wang, L.; Agrawalla, B. K.; Park, S.; Zhu, H.; Sivaraman, B.; Peng, J.; Xu, Q.; Chang, Y. *J. Am. Chem. Soc.* **2015**, *137*, 5930–5938.
(13) Xiao, H.; Xin, K.; Dou, H.; Yin, G.; Quan, Y.; Wang, R. *Chem. Commun.* **2015**, *51*, 1442–1445.
(14) Xiao, H.; Li, J.; Zhao, J.; Yin, G.; Quan, Y.; Wang, J.; Wang, R. *J. Mater. Chem. B* **2015**, *3*, 1633–1638.
(15) Hou, J.; Wu, M.; Li, K.; Yang, J.; Yu, K.; Xie, Y.; Yu, X. *Chem. Commun.* **2014**, *50*, 8640–8643.
(16) Li, G.; Lin, Q.; Ji, L.; Chao, H. *J. Mater. Chem. B* **2014**, *2*, 7918–7926.
(17) Li, D.; Feng, Y.; Lin, J.; Chen, M.; Wang, S.; Wang, X.; Sheng, H.; Shao, Z.; Zhu, M.; Meng, X. *Sens. Actuators, B* **2016**, *222*, 483–491.
(18) Hawkins, C. L.; Davies, M. J. *Chem. Res. Toxicol.* **2005**, *18*, 1600–1610.

DOI: 10.1021/acs.analchem.6b04094
Anal. Chem. 2017, 89, 1787–1792

(19) Yu, F.; Song, P.; Li, P.; Wang, B.; Han, K. *Chem. Commun.* **2012**, *48*, 7735−7737.
(20) Wang, B.; Li, P.; Yu, F.; Chen, J.; Qu, Z.; Han, K. *Chem. Commun.* **2013**, *49*, 5790−5792.
(21) Xu, K.; Luan, D.; Wang, X.; Hu, B.; Liu, X.; Kong, F.; Tang, B. *Angew. Chem., Int. Ed.* **2016**, *55*, 12751−12754.
(22) McCall, A. S.; Cummings, C. F.; Bhave, G.; Vanacore, R.; Page-McCaw, A.; Hudson, B. G. *Cell* **2014**, *157*, 1380−1392.
(23) Beija, M.; Afonso, C. A. M.; Martinho, J. M. G. *Chem. Soc. Rev.* **2009**, *38*, 2410−2433.
(24) Tang, B.; Yu, F.; Li, P.; Tong, L.; Duan, X.; Xie, T.; Wang, X. *J. Am. Chem. Soc.* **2009**, *131*, 3016−3023.
(25) Yuan, L.; Lin, W.; Yang, Y.; Chen, H. *J. Am. Chem. Soc.* **2012**, *134*, 1200−1211.
(26) Xu, K.; Qiang, M.; Gao, W.; Su, R.; Li, N.; Gao, Y.; Xie, Y.; Kong, F.; Tang, B. *Chem. Sci.* **2013**, *4*, 1079−1086.
(27) Wang, F.; Zhou, L.; Zhao, C.; Wang, R.; Fei, Q.; Luo, S.; Guo, Z.; Tian, H.; Zhu, W. *Chem. Sci.* **2015**, *6*, 2584−2589.
(28) Shao, X.; Kang, R.; Zhang, Y.; Huang, Z.; Peng, F.; Zhang, J.; Wang, Y.; Pan, F.; Zhang, W.; Zhao, W. *Anal. Chem.* **2015**, *87*, 399−405.
(29) Fidler, A. L.; Vanacore, R. M.; Chetyrkin, S. V.; Pedchenko, V. K.; Bhave, G.; Yin, V. P.; Stothers, C. L.; Rose, K. L.; McDonald, W. H.; Clark, T. A.; Borza, D. B.; Steele, R. E.; Ivy, M. T.; Hudson, J. K.; Hudson, B. G. *Proc. Natl. Acad. Sci. U. S. A.* **2014**, *111*, 331−336.

DOI: 10.1021/acs.analchem.6b04094
Anal. Chem. 2017, 89, 1787−1792